Reactions of Neutral Co(II) Complexes of a Dianionic Tetrapodal Pentadentate Ligand: Co(III) Amides from Imido Radicals.

Lucie Nurdin,[†]Denis M. Spasyuk,[†,‡] Warren E. Piers,[†] and Laurent Maron*[§]*

[†]Department of Chemistry, University of Calgary, 2500 University Dr. NW, Calgary, AB, Canada T2N 1N4.

§LPCNO, Université de Toulouse, INSA, UPS, LPCNO, 135 avenue de Rangueil, F- 31077 Toulouse, France, and CNRS, LPCNO, F-31077 Toulouse, France.

[‡]Canadian Light Source Inc. 44 Innovation Boulevard, Saskatoon, Saskatchewan, Canada SK S7N 2V3.

Supporting Information

Table of Contents

Experimental Details.

General. Unless mentioned otherwise, all manipulations were performed under an inert gas (argon) in gloveboxes or using standard Schlenk techniques. All anhydrous solvents were prepared by passing through Mbraun SP-800 solvent purification system and were stored in 500 mL thick-walled vessels over sodium/benzophenone ketal or CaH_2. All dried solvents were degassed and vacuum distilled prior to use. Pentane, hexanes and benzene solvents were dried over K/Na alloy and freshly distilled before use. Me_3SnCl was purchased from TCI. All other chemicals were obtained from Sigma Aldrich and used as received. Adamantyl azide was obtained from Sigma-aldrich and store in the freezer (-36 °C). 1-azido-4-tert-butylbenzene,[1] 4-tert-butylbenzenesulfonyl azide,[2] and 3,5-bis-(trifluoromethyl)phenyl azide[3] were prepared by literature procedures. All azides were stored in the freezer (-36 °C). The synthesis of the dianionic pentadentate ligand has previously been reported.[4]

Physical Methods

^1H, $^{13}C\{^1H\}$ chemical shifts are referenced to the residual solvent signals of THF (^1H, 5.02, 3.88 ppm; $^{13}C\{^1H\}$, 67.21, 25.31 ppm), C_6D_6 (^1H, 7.16 ppm; $^{13}C\{^1H\}$, 128.06 ppm) and CD_2Cl_2 (^1H, 5.12 ppm; $^{13}C\{^1H\}$, 53.84 ppm). ^1H, $^{13}C\{^1H\}$, ^{19}F, ^1H-^1H-COSY, ^1H-^{13}C-HSQC and ^1H-^{13}C-HMBC NMR experiments were performed at room temperature on Bruker RDQ-400, or Ascend-500 or Avance-600 MHz spectrometers and analysed with MestReNova software (v8.1, Mestrelab Research S.L.). All ^{11}B chemical shifts are relative to $BF_3{\cdot}OEt_2$, all ^{19}F chemical shifts are relative to hexafluorobenzene. X-ray crystallographic analyses were performed on Cu Kα radiation on a Bruker Smart diffractometer equipped with Apex II detector, fixed-CHI goniometer, and sealed-tube (Cu) source or with Mo Kα radiation on a Nonius Kappa CCD diffractometer with samples coated in Paratone 8277 oil (Exxon) and mounted on a glass fibre. Full crystallography details can be found in independently uploaded .cif files. Elemental analysis was performed on site by Johnson Li using a Perkin Elmer Model 2400 series II analyzer. Infra-red spectra were collected on a Nicolet Avatar FT-IR spectrometer, and samples were prepared as a thin film by solution evaporation (benzene) on NaCl or AgCl plates, sealed with Parafilm. Solution high resolution-mass spectrometry experiments were performed on a Kratos MS-80 spectrometer by Wade White (direct ESI-MS or APCI-MS) on samples prepared in the glove box in a gas tight syringe. Absorption spectra were measured using a Varian Cary-50 single beam

spectrophotometer. The solutions were placed in a co-joint UV-vis cuvette of 2 mm path length. Epsilon values were estimated from one UV-vis spectrum. Cyclic voltammetry experiments were carried out using CH instrument potentiostat and C-3 cell stand. A platinum working electrode, a platinum counter electrode and a silver wire pseudo reference electrode were used for cyclic voltammetry experiments in CH_3CN with 0.1 M $[Bu_4N][PF_6]$ electrolyte in a glovebox. Ferrocene ($E_{Fc+/0}$ = 0.64 V vs SHE) was added during each experiment as an internal reference. X-band EPR spectra were recorded on a Bruker EMX 10/12 spectrometer equipped with a VT capabilities with a 10 inch magnet and a 12 kV power supply. For EPR studies, dry degassed toluene was used as the solvent. Samples were prepared by dissolving 0.001 mmol of compound in 1 mL of toluene to which 100 equivalents of the azide was added. All manipulations were carried out inside a glove box. Amp. mod: 10 G.

Computational Details

All the quantum-chemical calculations were conducted using the Gaussian09 program suite.* As functional we have used the Becke's 3-parameter hybrid one,[4] combined with the non-local correlation functional provided by Perdew/Wang, denoted as B3PW91.[5] For Co, the relativistic energy-consistent pseudopotential of the Stuttgart-Köln ECP library was used in combination with its adapted segmented basis.[6] For all other atoms, a standard 6-31G** basis set was used.[7, 8] All stationary points have been identified as minima (number of imaginary frequencies Nimag=0) or transition states (Nimag=1) and IRC calculations were carried out from all transition states.

* Gaussian 09, Revision A.02, M. J. Frisch, G. W. Trucks, H. B. Schlegel, G. E. Scuseria, M. A. Robb, J. R. Cheeseman, G. Scalmani, V. Barone, B. Mennucci, G. A. Petersson, H. Nakatsuji, M. Caricato, X. Li, H. P. Hratchian, A. F. Izmaylov, J. Bloino, G. Zheng, J. L. Sonnenberg, M. Hada, M. Ehara, K. Toyota, R. Fukuda, J. Hasegawa, M. Ishida, T. Nakajima, Y. Honda, O. Kitao, H. Nakai, T. Vreven, J. A. Montgomery, Jr., J. E. Peralta, F. Ogliaro, M. Bearpark, J. J. Heyd, E. Brothers, K. N. Kudin, V. N. Staroverov, R. Kobayashi, J. Normand, K. Raghavachari, A. Rendell, J. C. Burant, S. S. Iyengar, J. Tomasi, M. Cossi, N. Rega, J. M. Millam, M. Klene, J. E. Knox, J. B. Cross, V. Bakken, C. Adamo, J. Jaramillo, R. Gomperts, R. E. Stratmann, O. Yazyev, A. J. Austin, R. Cammi, C. Pomelli, J. W. Ochterski, R. L. Martin, K. Morokuma, V. G. Zakrzewski, G. A. Voth, P. Salvador, J. J. Dannenberg, S. Dapprich, A. D. Daniels, O. Farkas, J. B. Foresman, J. V. Ortiz, J. Cioslowski, D. J. Fox, Gaussian, Inc., Wallingford CT, **2009**.

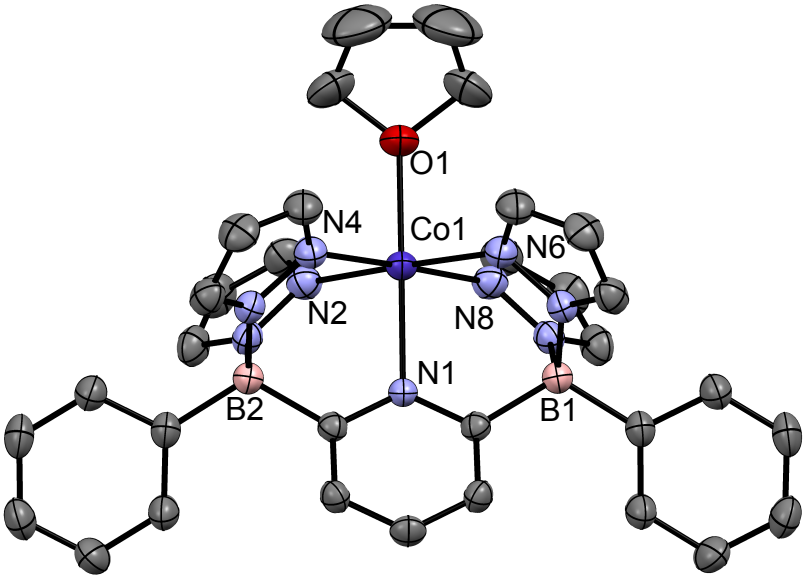

Figure S1. ORTEP diagrams for **1-THF.** Thermal ellipsoids are shown at the 50% probability level. Calculated hydrogen atoms are omitted for clarity. Selected bond distances (Å): Co1-N2, 2.148(2); Co1-N4, 2.082(2); Co1-N1, 2.135(3); Co1-O1, 2.164(3). Selected bond angles (°): N2-Co1-N4, 84.65(9); N1-Co1-O1, 174.6(1).

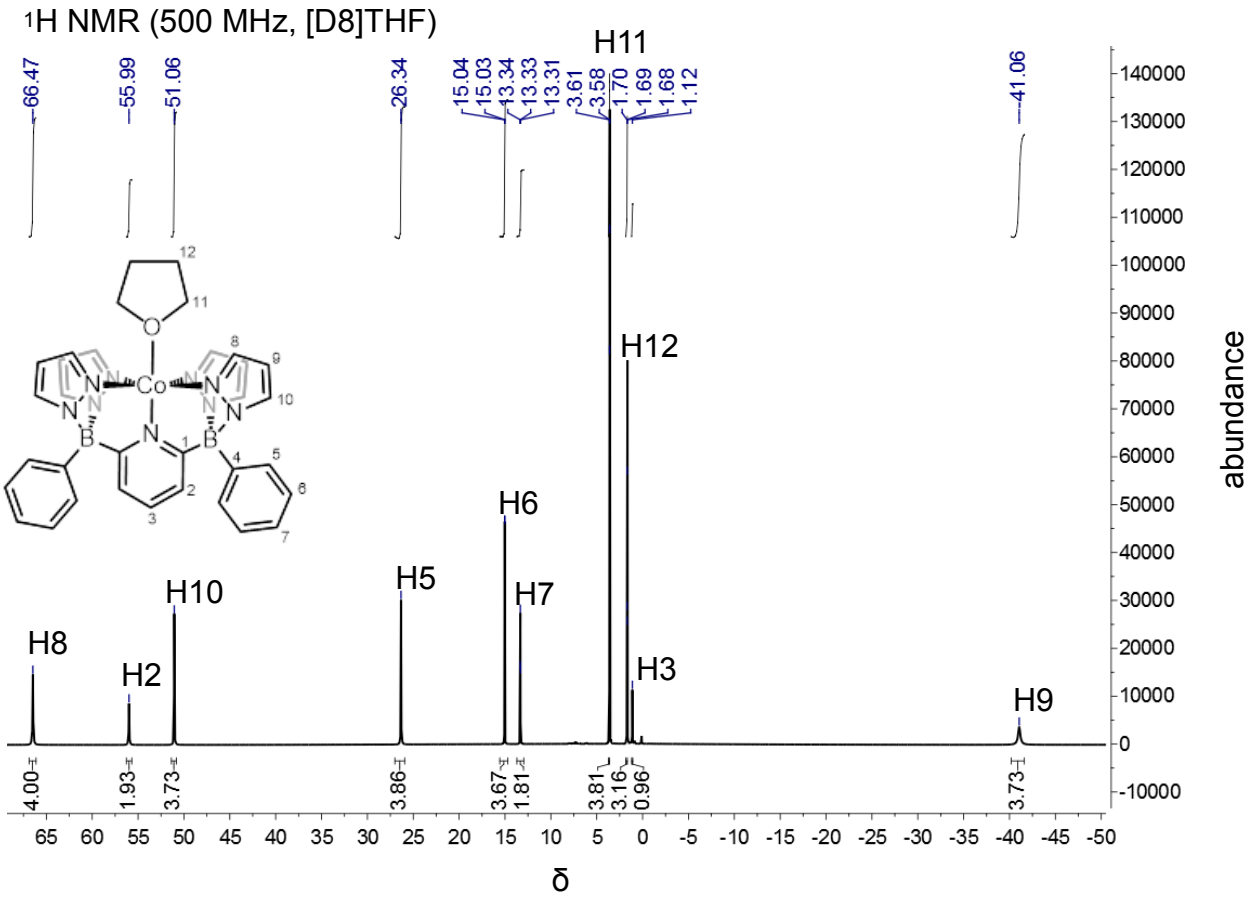

Figure S2. ^{1}H NMR spectrum of **1-THF** in [D8]THF.

A.

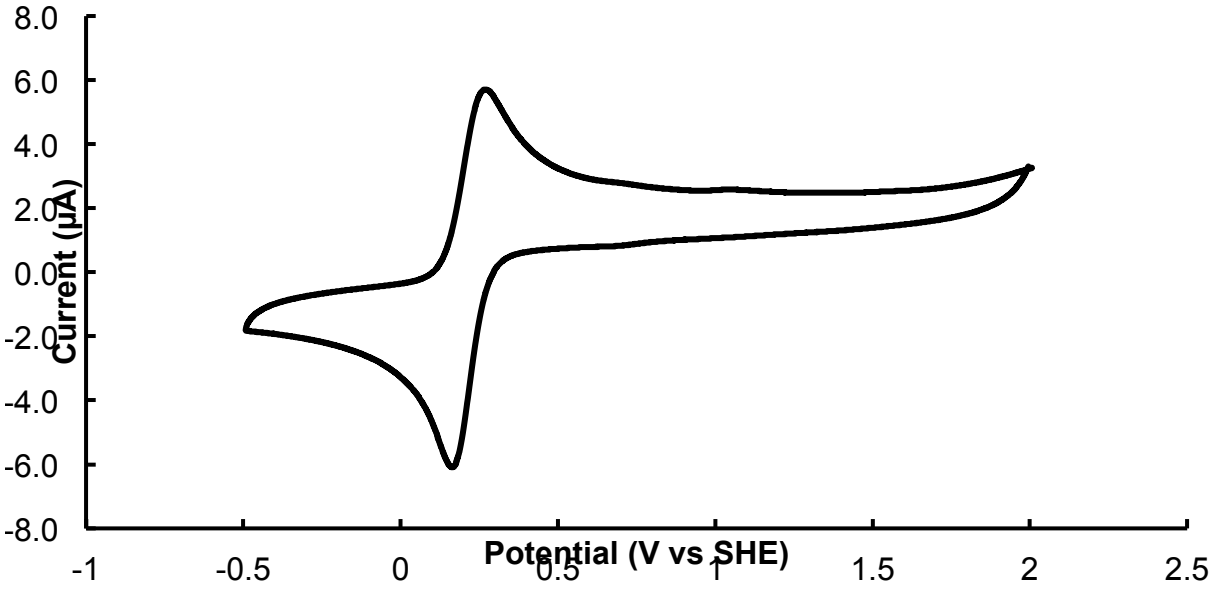

B.

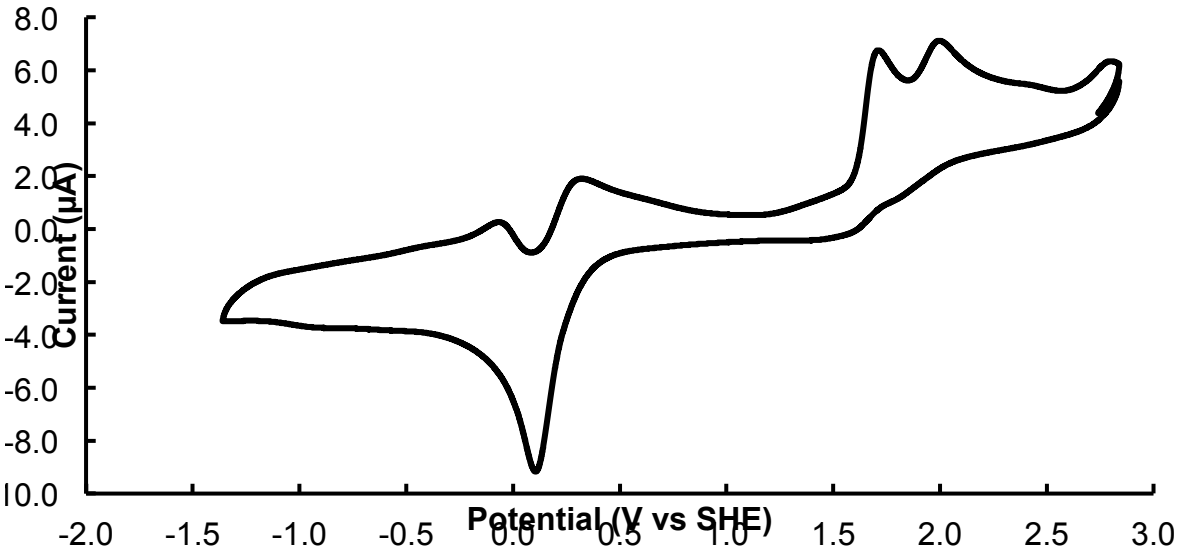

Figure S3. Refer to physical method for general information. **A.** Cyclic voltammogram of **1-THF** in CH_3CN (Concentration of **1-THF**: 0.1 mM). (Scan rate: 100 mV/s). **B.** Cyclic voltammogram of $[B_2Pz_4LiPyH]_2$ in CH_3CN (Concentration of $[B_2Pz_4LiPyH]_2$: 0.1 mM). (Scan rate: 100 mV/s). The two irreversible oxidation waves at + 1.71 V and + 1.99 V vs SHE are likely due to oxidation of the borate moieties. The reduction wave at + 0.10 V vs SHE is likely arising from the reduction of the pyridinium salt followed by two oxidation waves at – 0.05 V and +0.32 V vs SHE probably due to dimerization process of the pyridinium.[9]

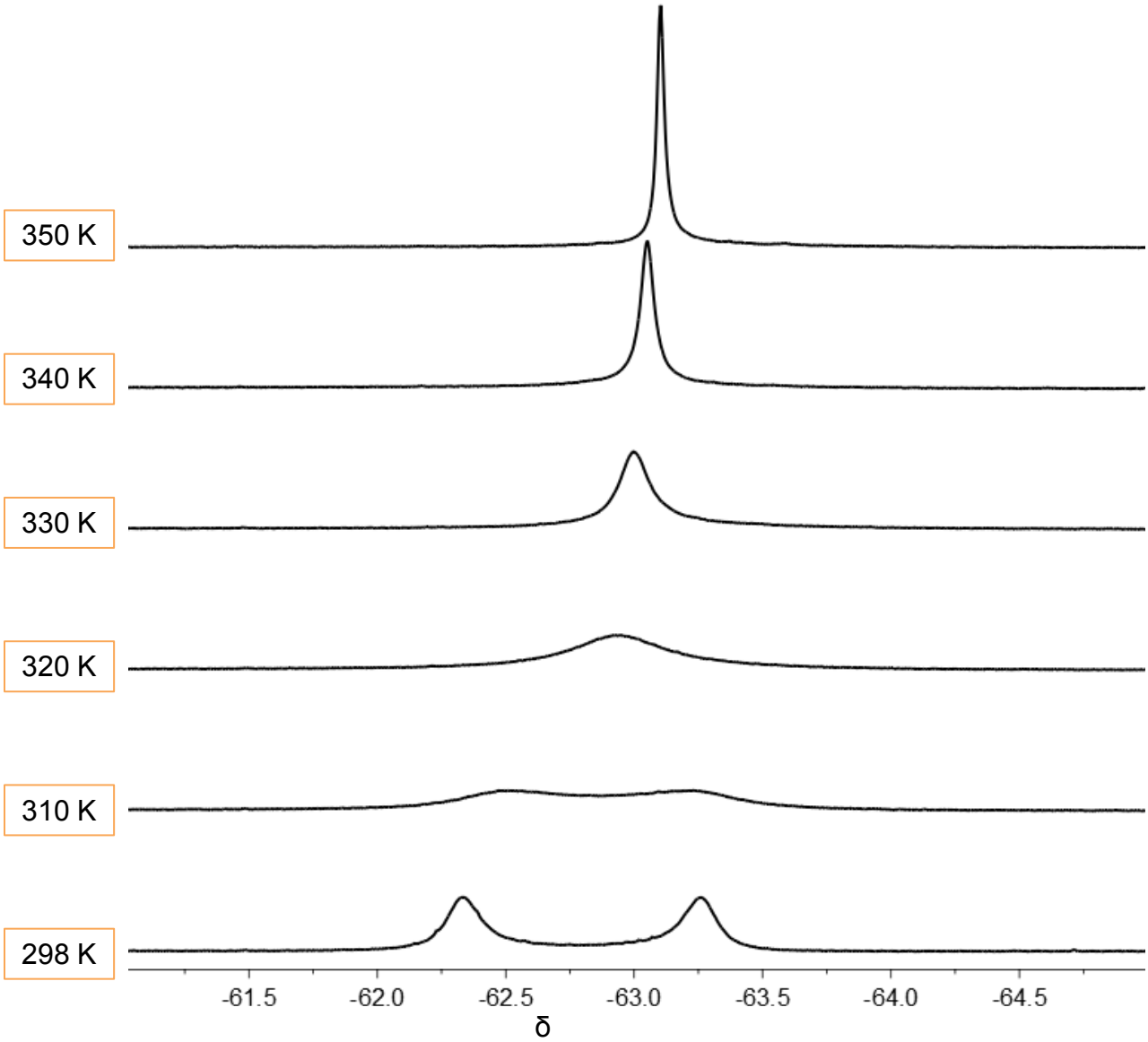

Figure S4. ^{19}F NMR spectra of **2-CF_3** in C_7D_8 at various temperatures. The coalescence is observed at 315 K.

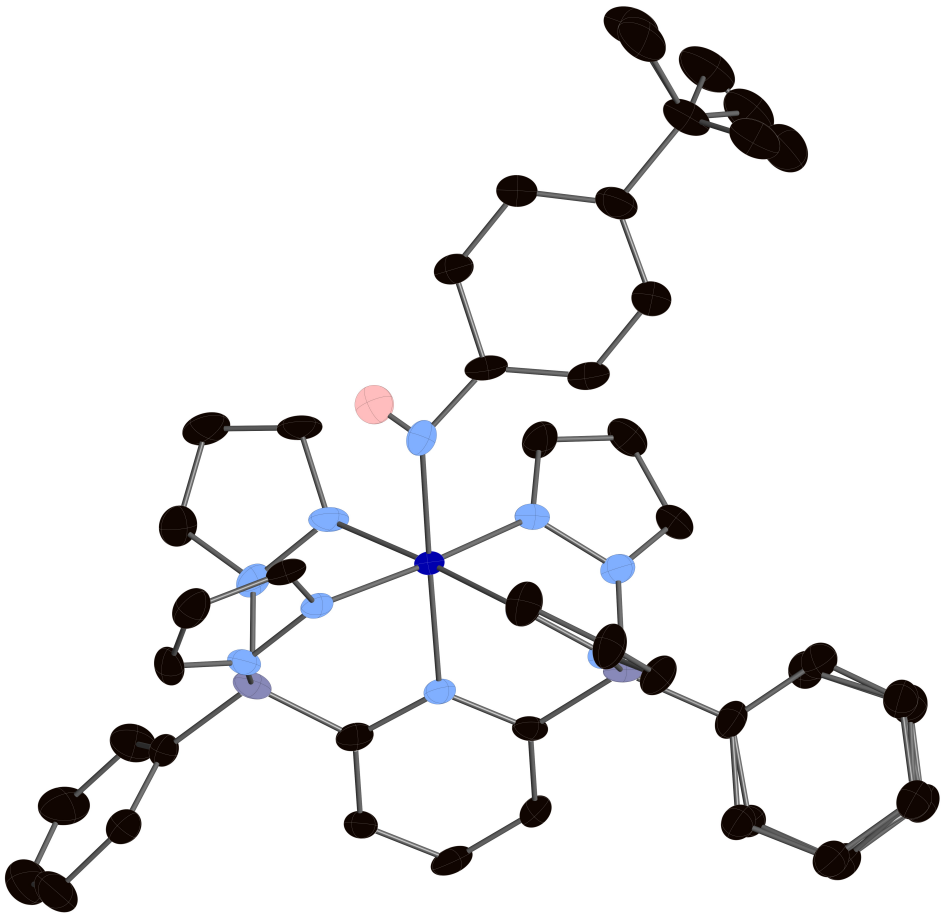

Figure S5. ORTEP diagrams for **2-tBu.** Thermal ellipsoids are shown at the 50% probability level. Calculated hydrogen atoms are omitted for clarity except the amido (N10) hydrogen. Due to a lack of precision in the data, the structure is only sufficient for establishing connectivity and no discussion of metrical parameters is warranted.

A.

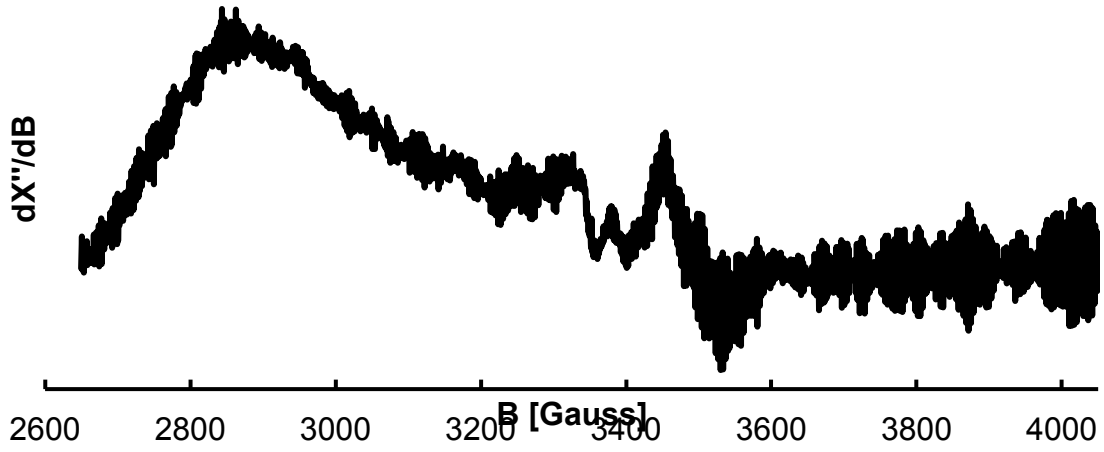

B.

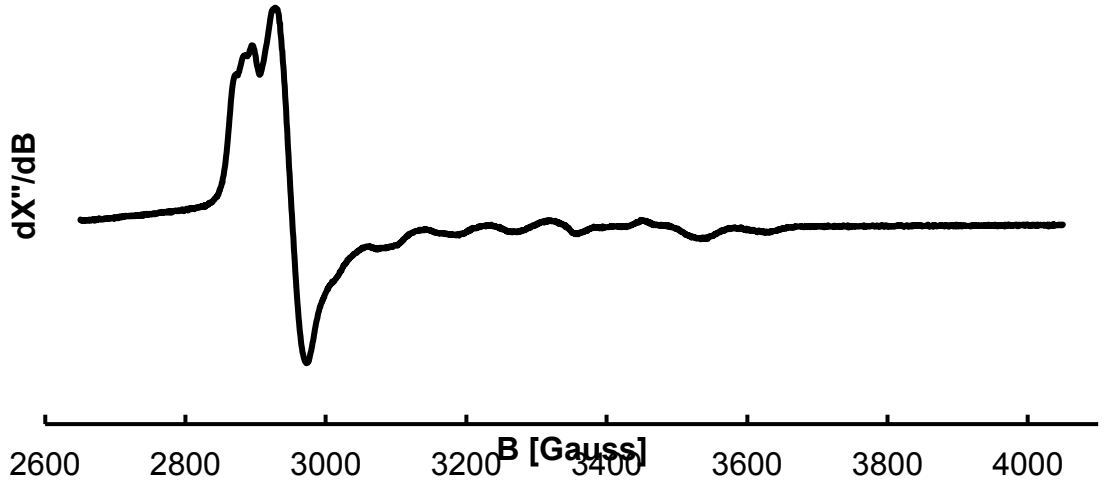

Figure S6. A. X-band EPR spectrum of **1** in toluene solution at room temperature. Experiment was run with a center field of 3350 G and a sweep width of 1400 G. The resolution was set to resolution in x2048, and the time constant and conversion time were set to 5.12 msec and 20.48 msec respectively. 16 scans were collected. Frequency: 9.388562 GHz. **B.** X-band EPR spectrum of **1** in toluene solution at 160 K. Experiment was run with a center field of 2940 G and a sweep width of 550 G. The resolution was set to resolution in x4096, and the time constant and conversion time were set to 2.56 msec and 10.24 msec respectively. 16 scans were collected. Frequency: 9.388563 GHz.

A.

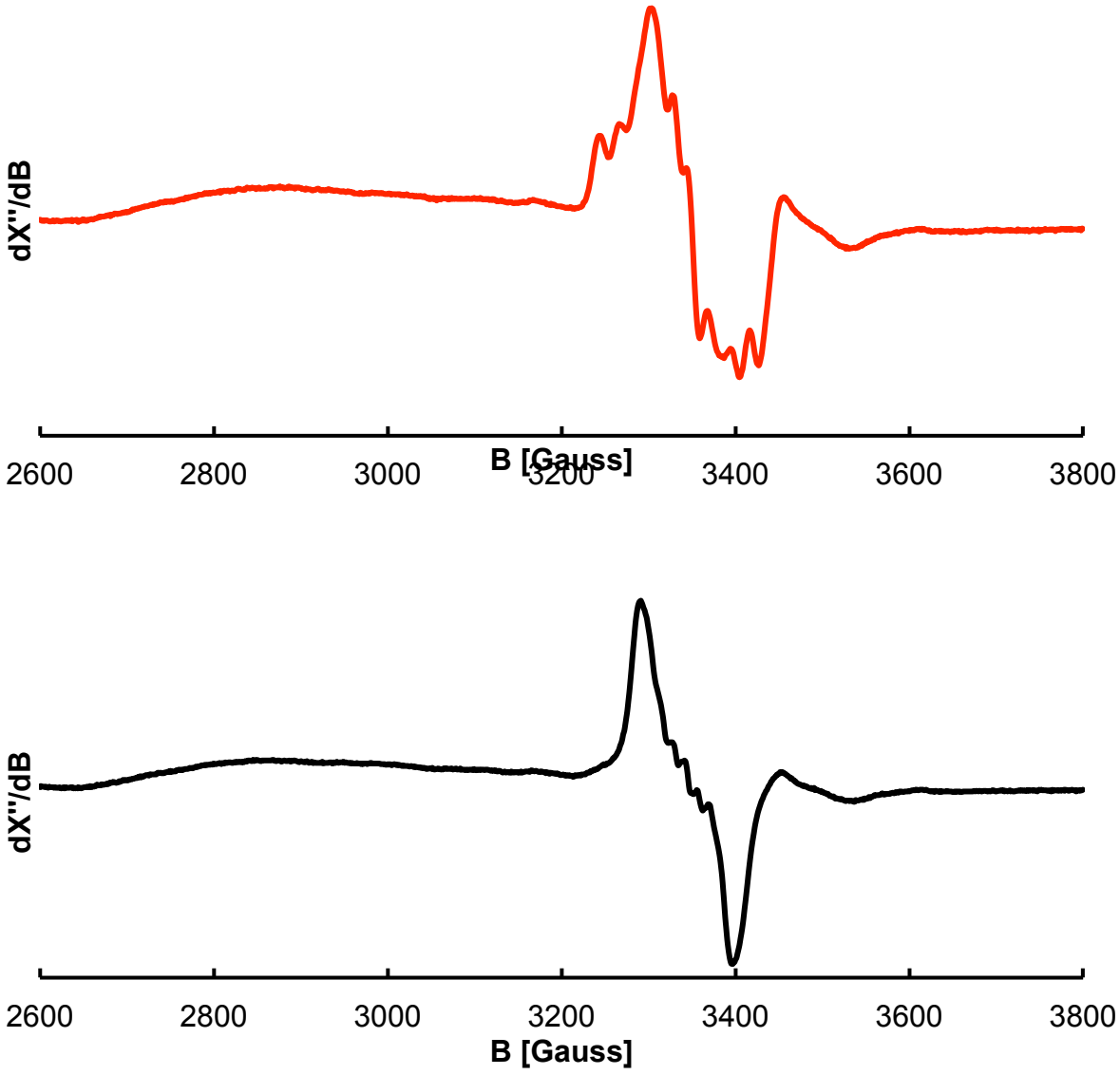
dX''/dB
2600
2800
3000
3200
3400
3600
3800
B [Gauss]
dX''/dB
2600
2800
3000
3200
3400
3600
3800
B [Gauss]

B.

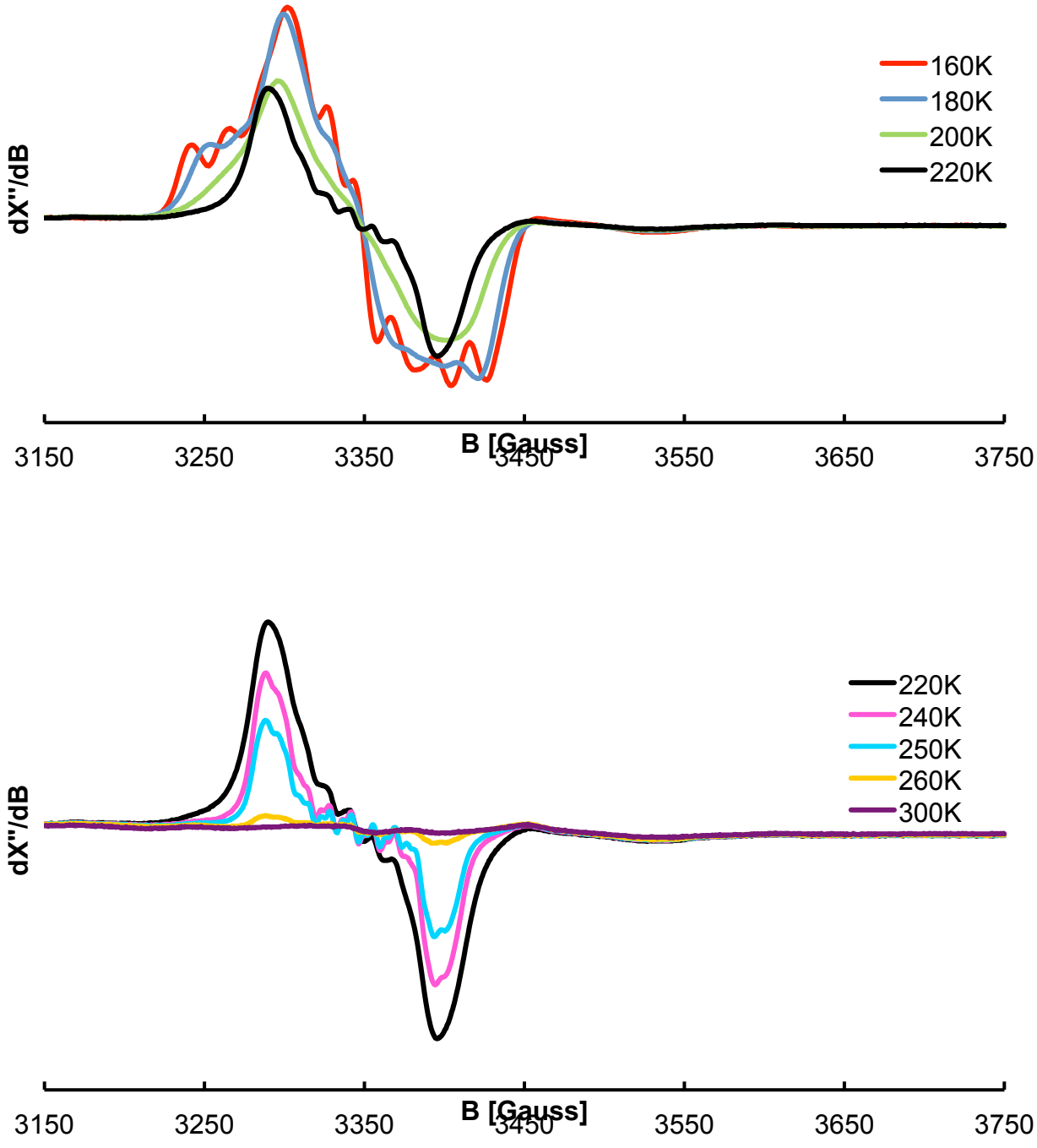

Figure S7. A. X-band EPR spectrum of **5-tBu** in toluene solution at 160 K (red) and 220 K (black) that shows the disappearance of **1**. Experiment was run with a center field of 3200 G and a sweep width of 1200 G. The resolution was set to resolution in x1024, and the time constant

and conversion time were set to 10.24 msec and 40.96 msec respectively. 8 scans were collected. Frequency: 9.386268 GHz. **B.** X-Band EPR spectra of **5-tBu** in toluene at various temperatures (two different figures made for clarity). Experiments were run with a center field of 3450 G and a sweep width of 600 G. The resolution was set to resolution in x1024, and the time constant and conversion time were set to 10.24 msec and 40.96 msec respectively. 8 scans were collected for each experiment. Frequency: 9.385005 GHz.

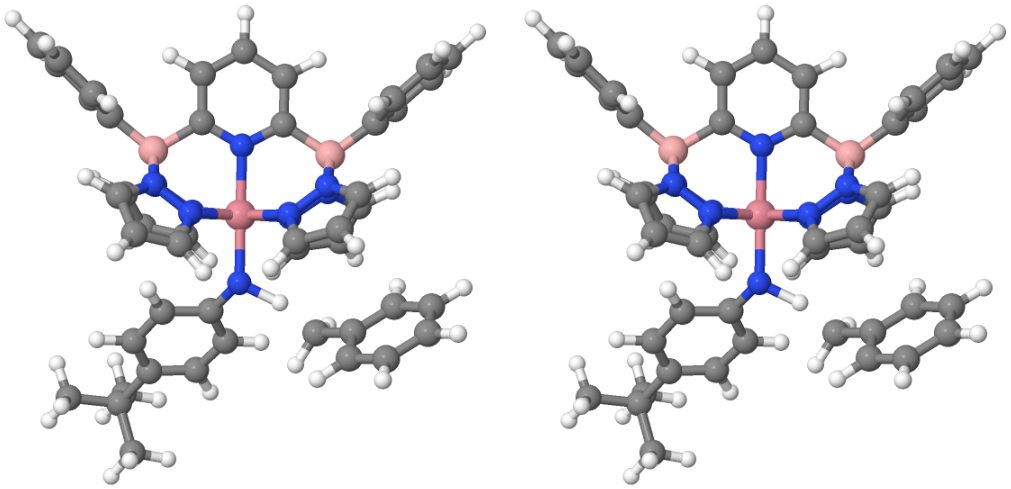

Figure S8. Geometries of the transition states for HAT from toluene (left) and CHD (right) to **5-tBu**.

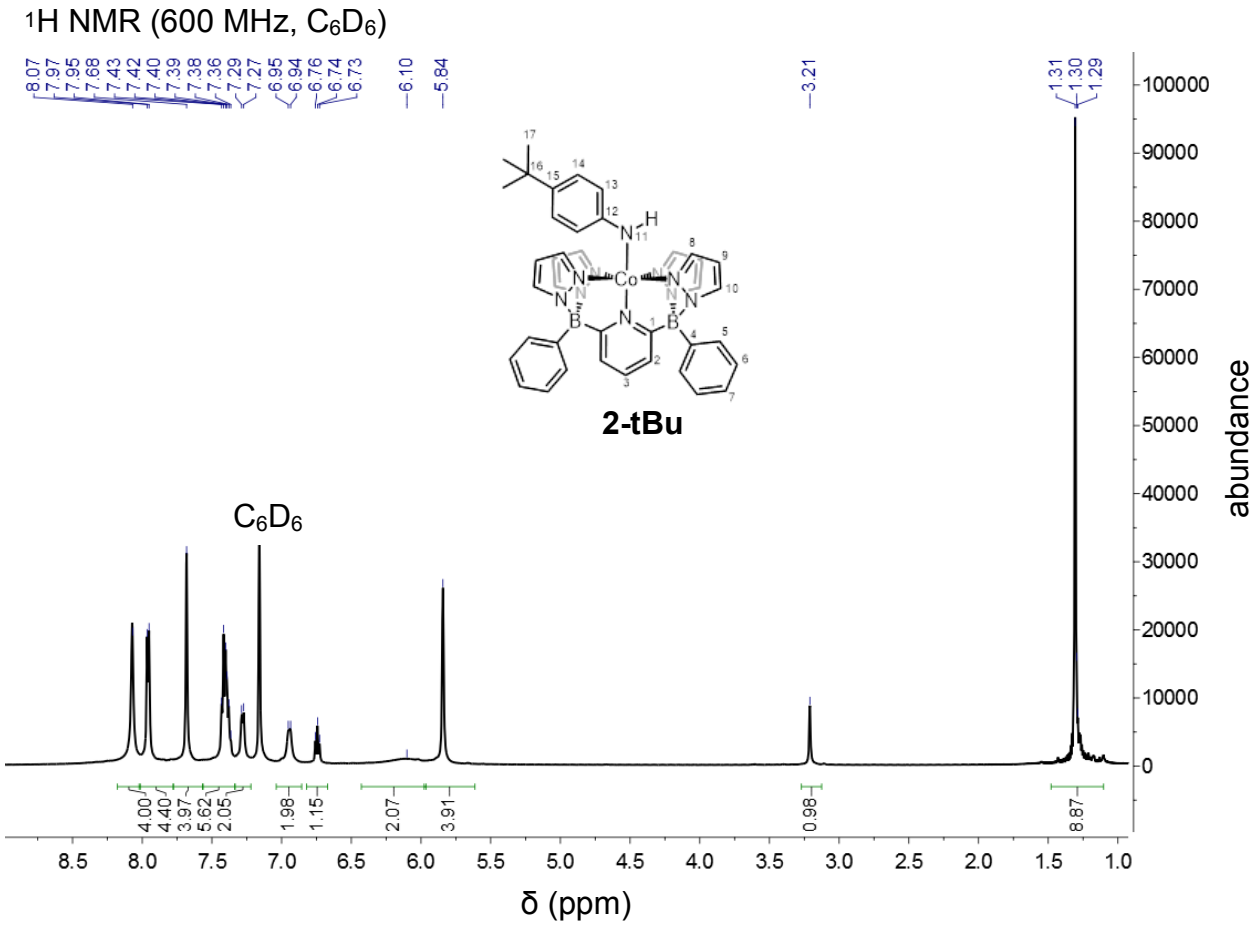

Figure S9. ^{1}H NMR spectrum of **2-tBu** in C_6D_6.

$^{13}C\{^{1}H\}$ NMR (151 MHz,

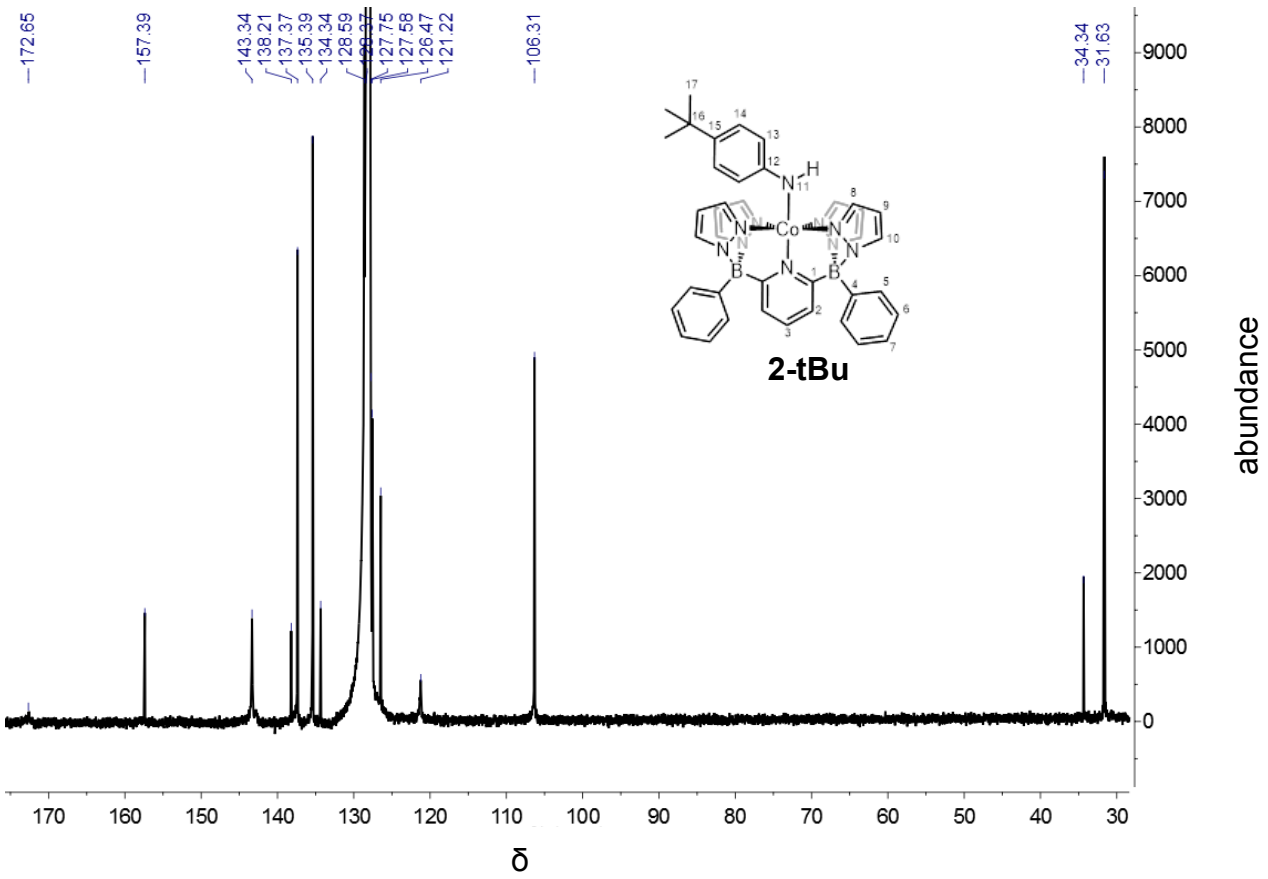

Figure S10. $^{13}C\{^{1}H\}$ NMR spectrum of **2-tBu** in C_6D_6.

^{1}H NMR (500 MHz, C_6D_6)

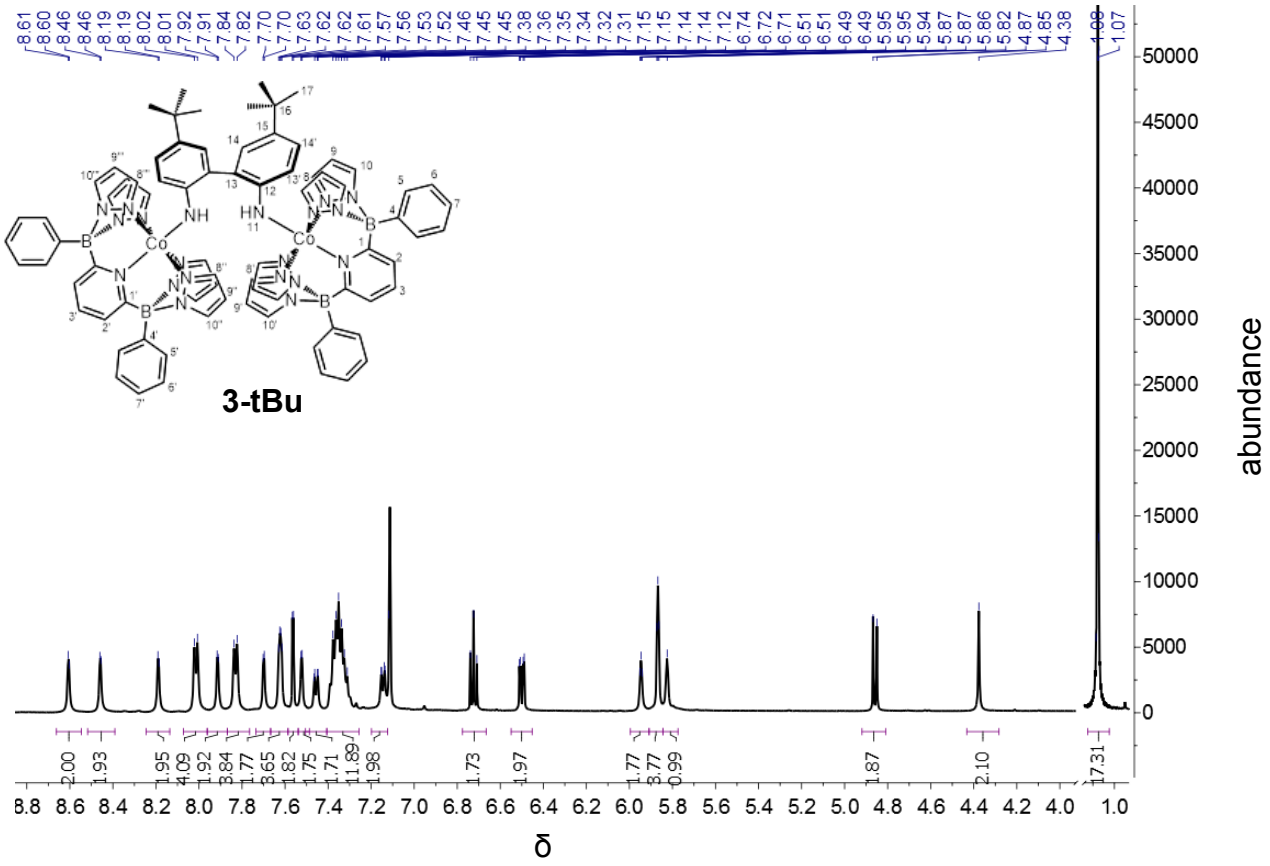

Figure S11. ^{1}H NMR spectrum of **3-tBu** in C_6D_6.

$^{13}C\{^{1}H\}$ NMR (126 MHz,

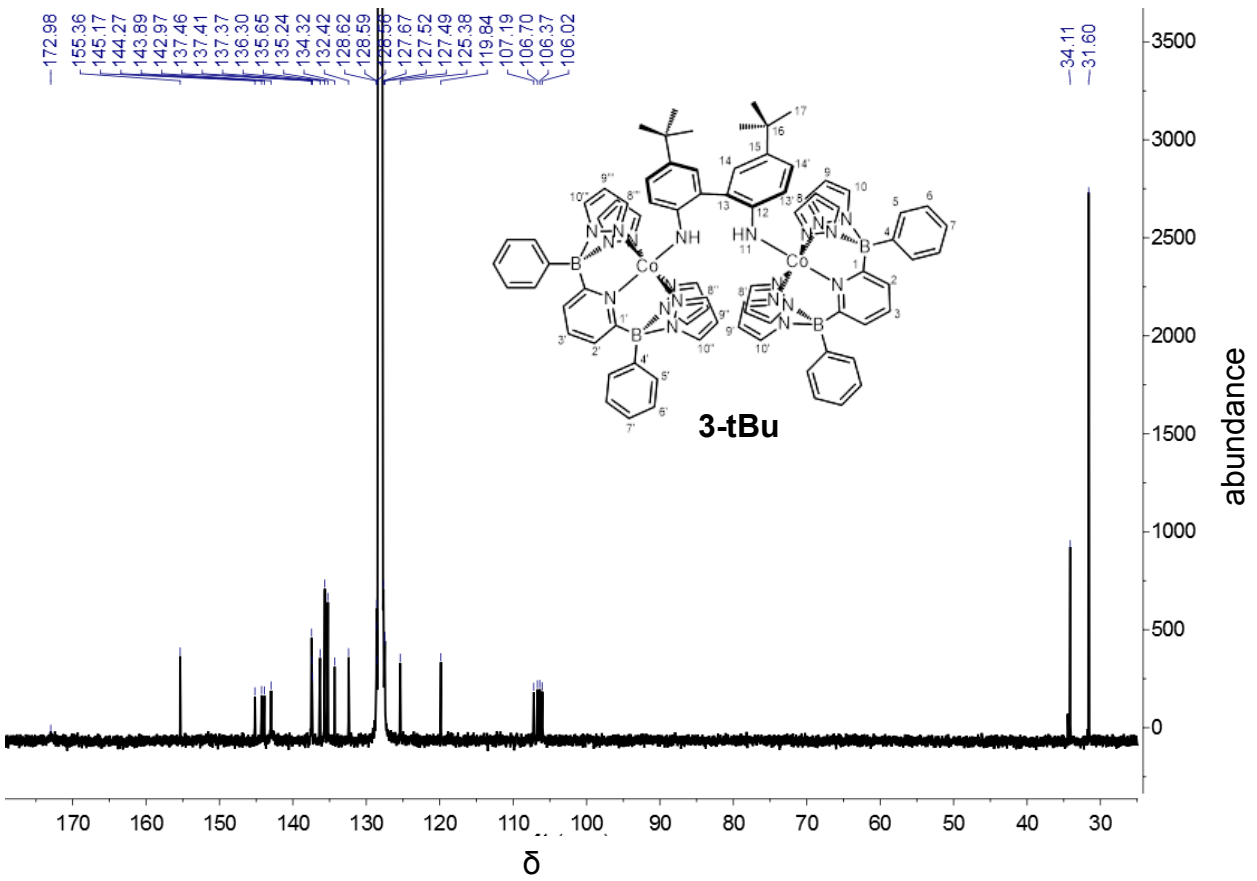

Figure S12. $^{13}C\{^{1}H\}$ NMR spectrum of **3-tBu** in C_6D_6.

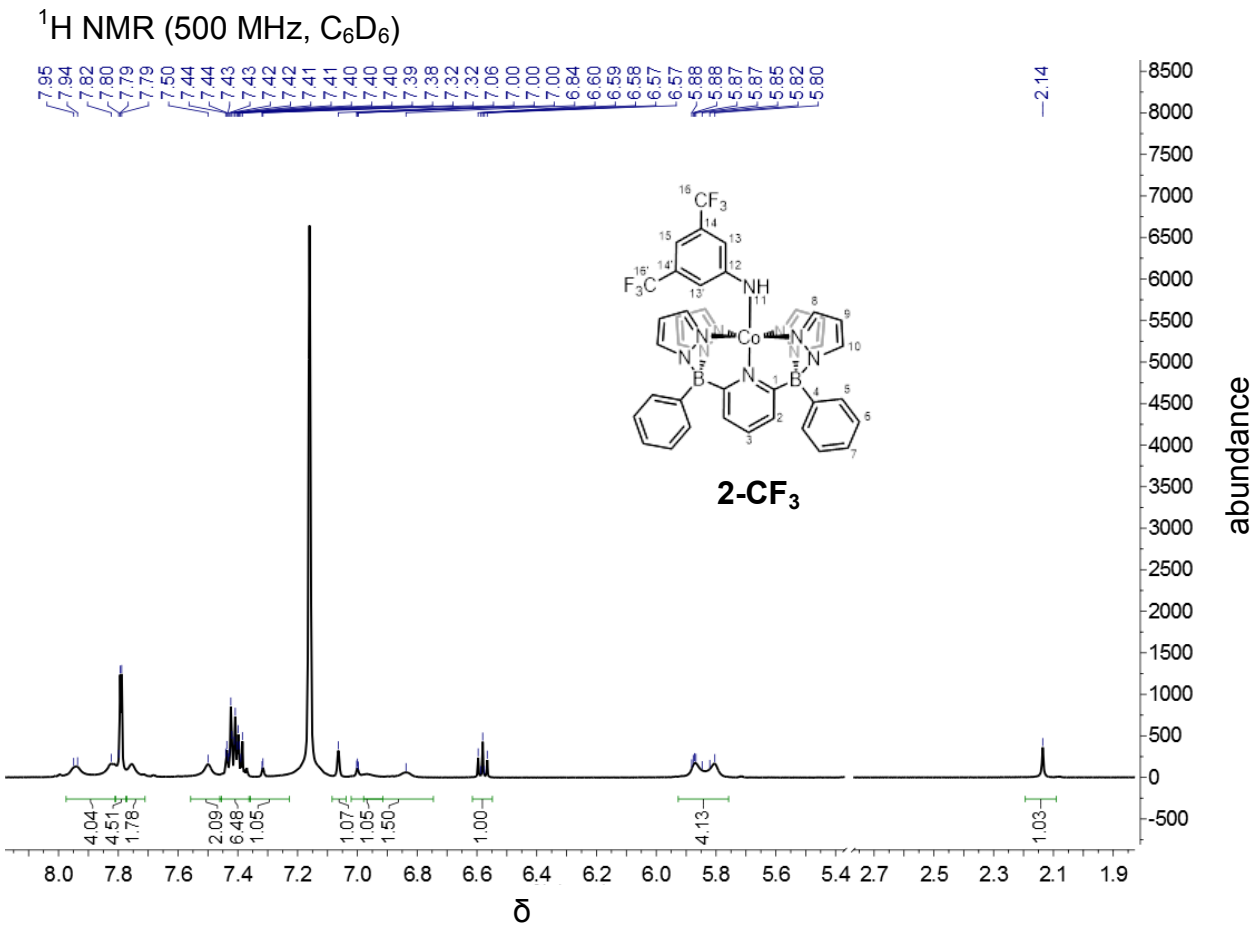

Figure S13. ^{1}H NMR spectrum of **2-CF$_3$** in C_6D_6.

$^{13}C\{^{1}H\}$ NMR (126 MHz,

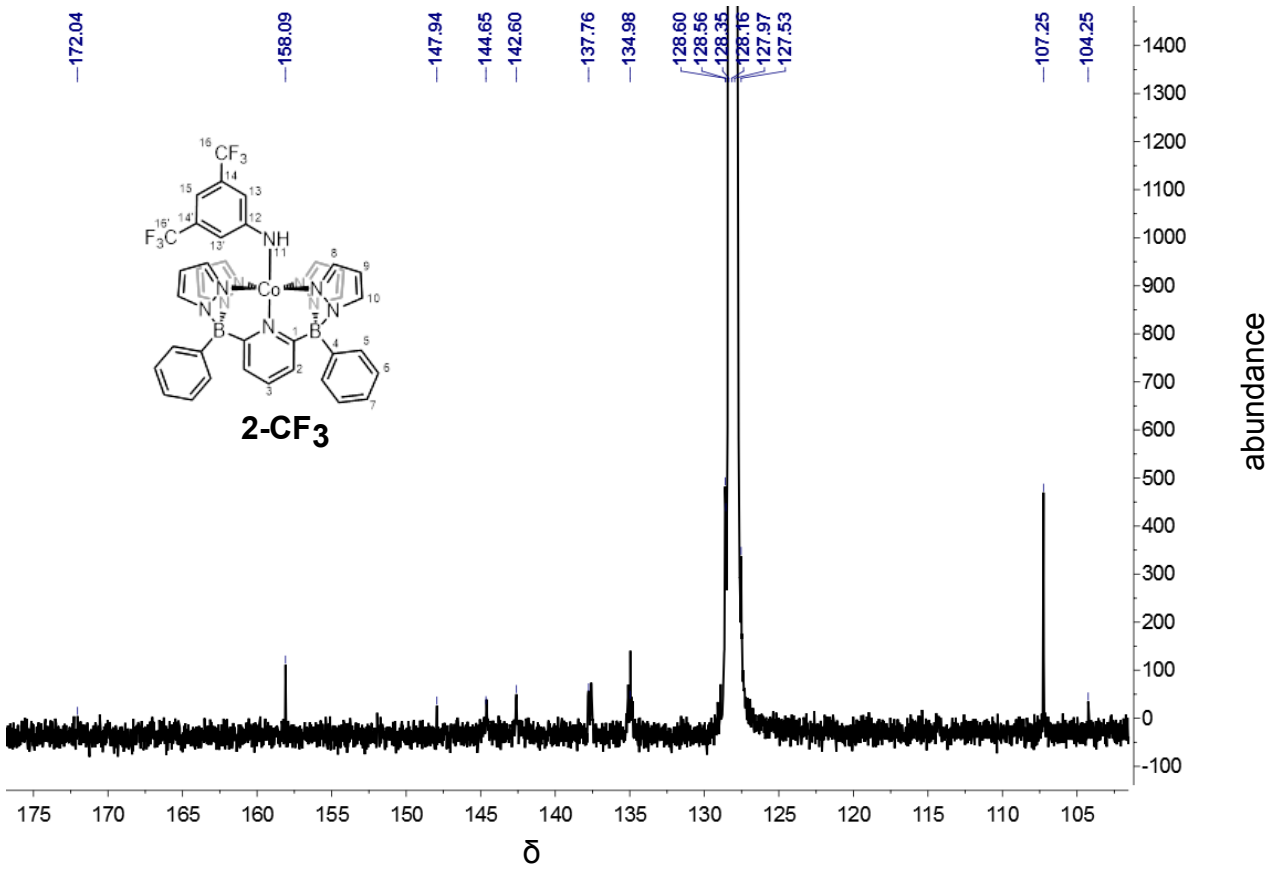

Figure S14. $^{13}C\{^{1}H\}$ NMR spectrum of **2-CF$_3$** in C_6D_6.

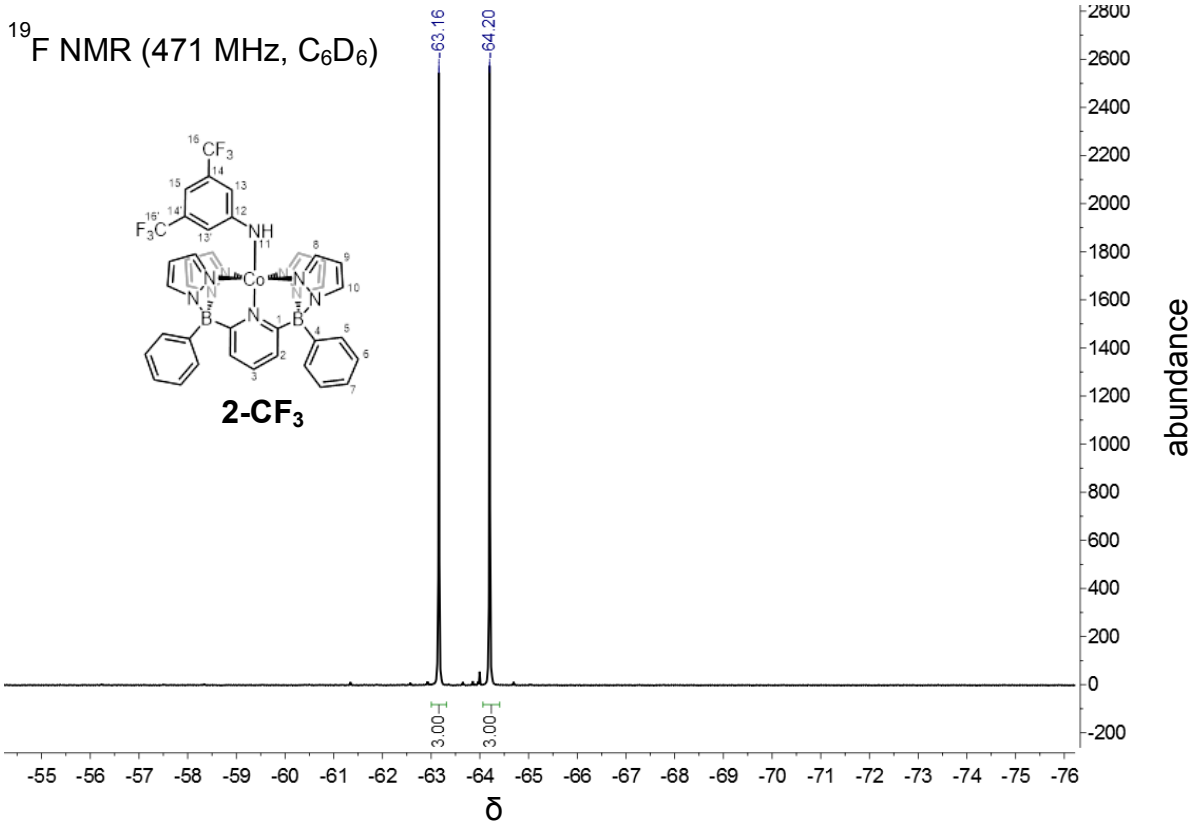

Figure S15. ^{19}F NMR spectrum of **2-CF_3** in C_6D_6.

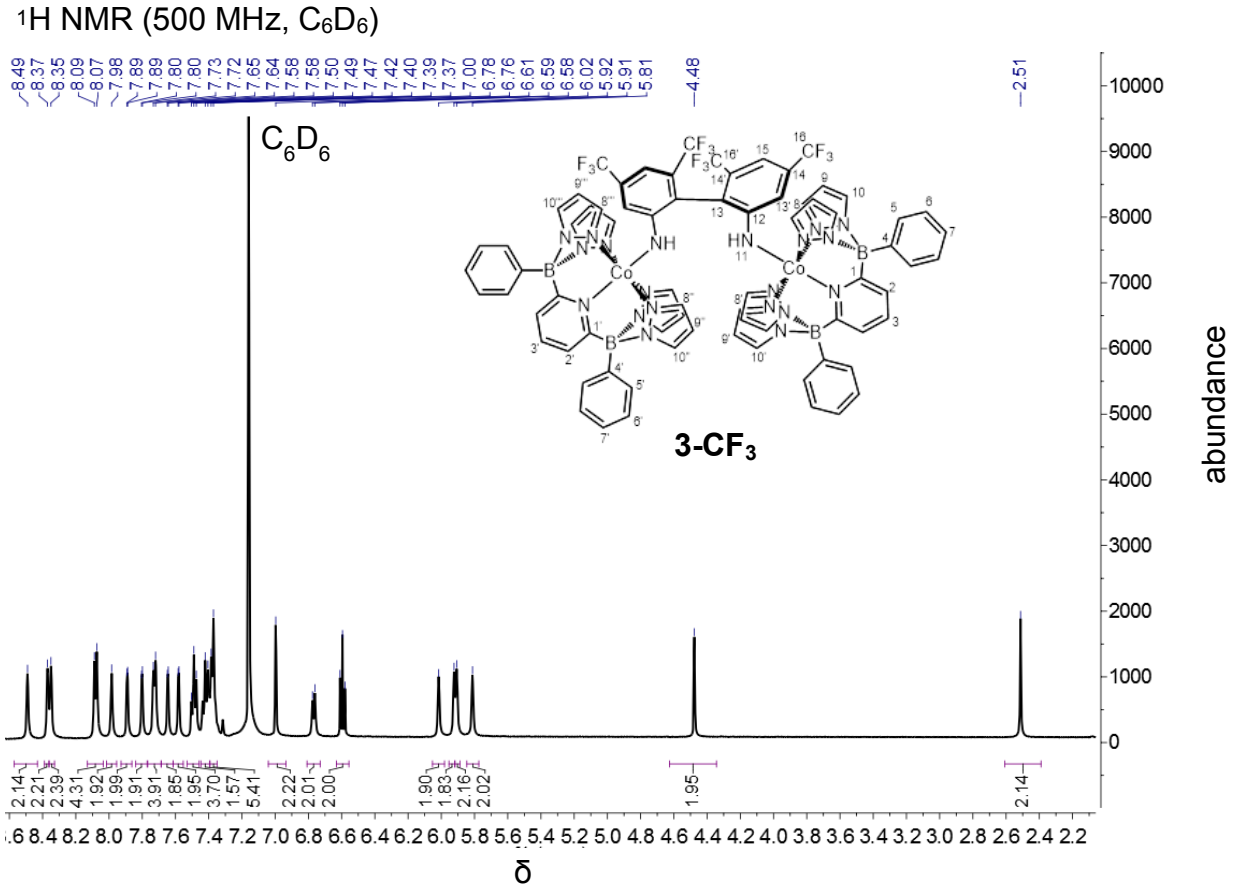

Figure S16. ^{1}H NMR spectrum of **3-CF$_3$** in C_6D_6.

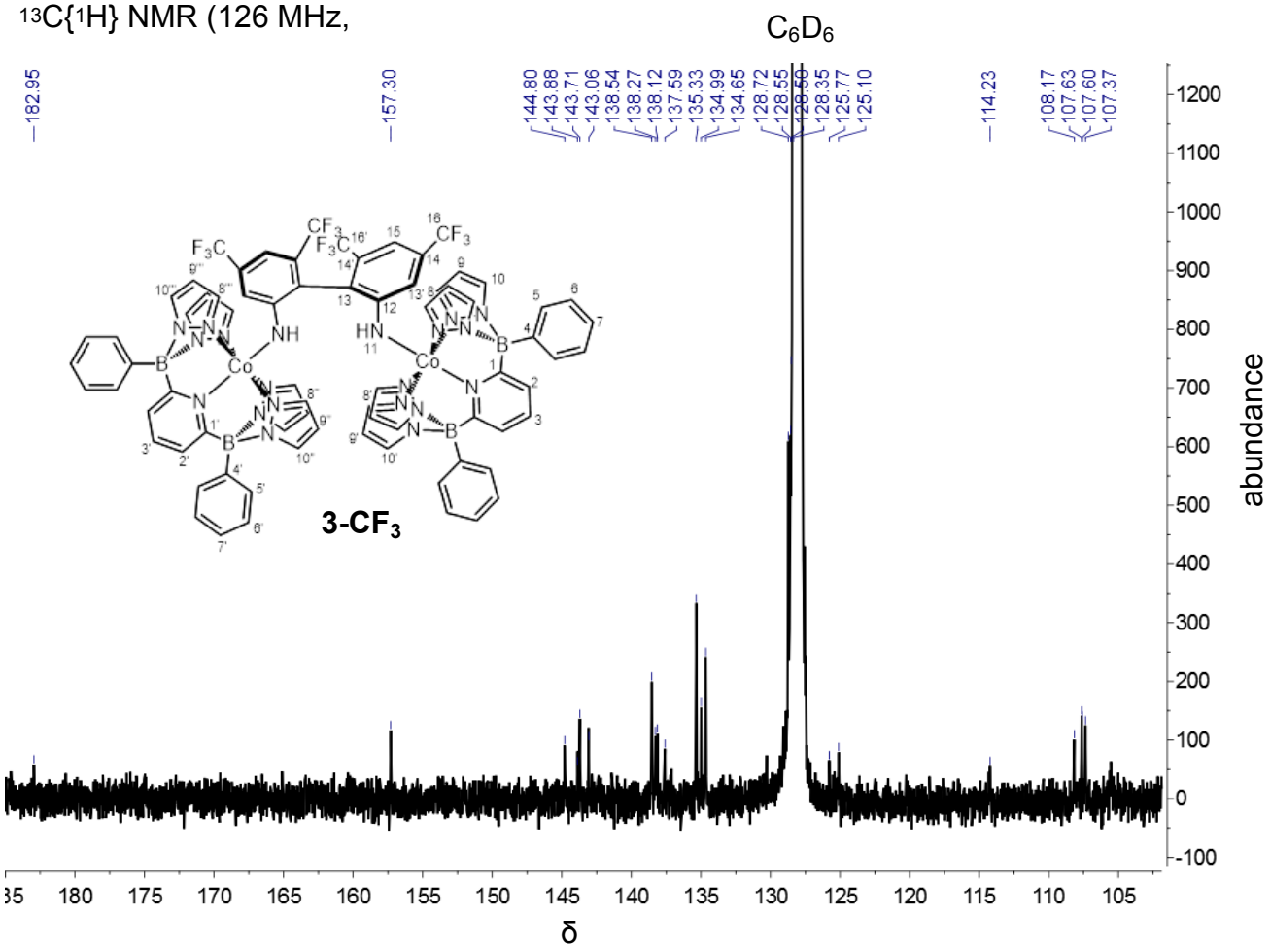

Figure S17. $^{13}C\{^{1}H\}$ NMR spectrum of **3-CF$_3$** in C_6D_6.

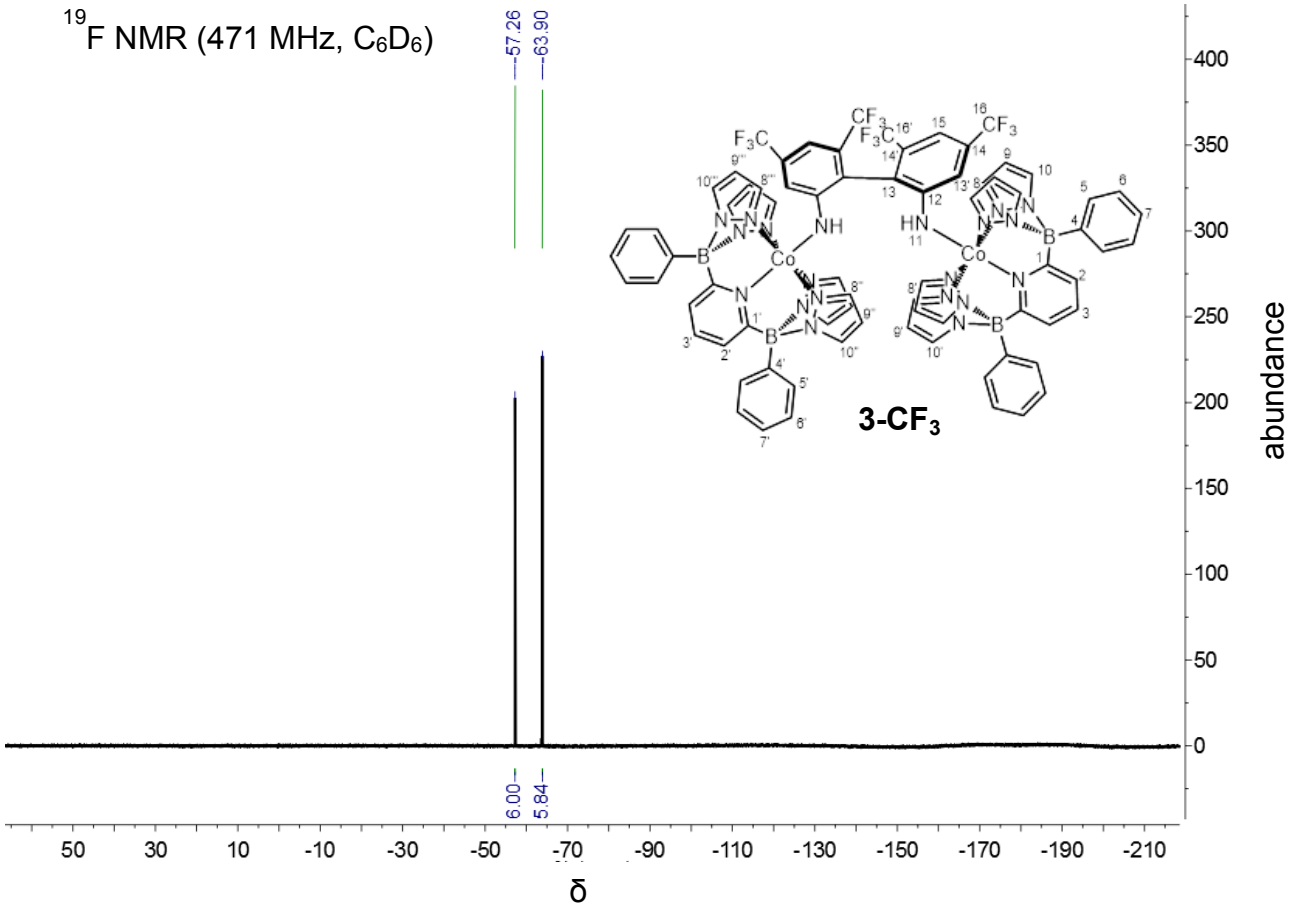

Figure S18. ^{19}F NMR spectrum of **3-CF$_3$** in C_6D_6.

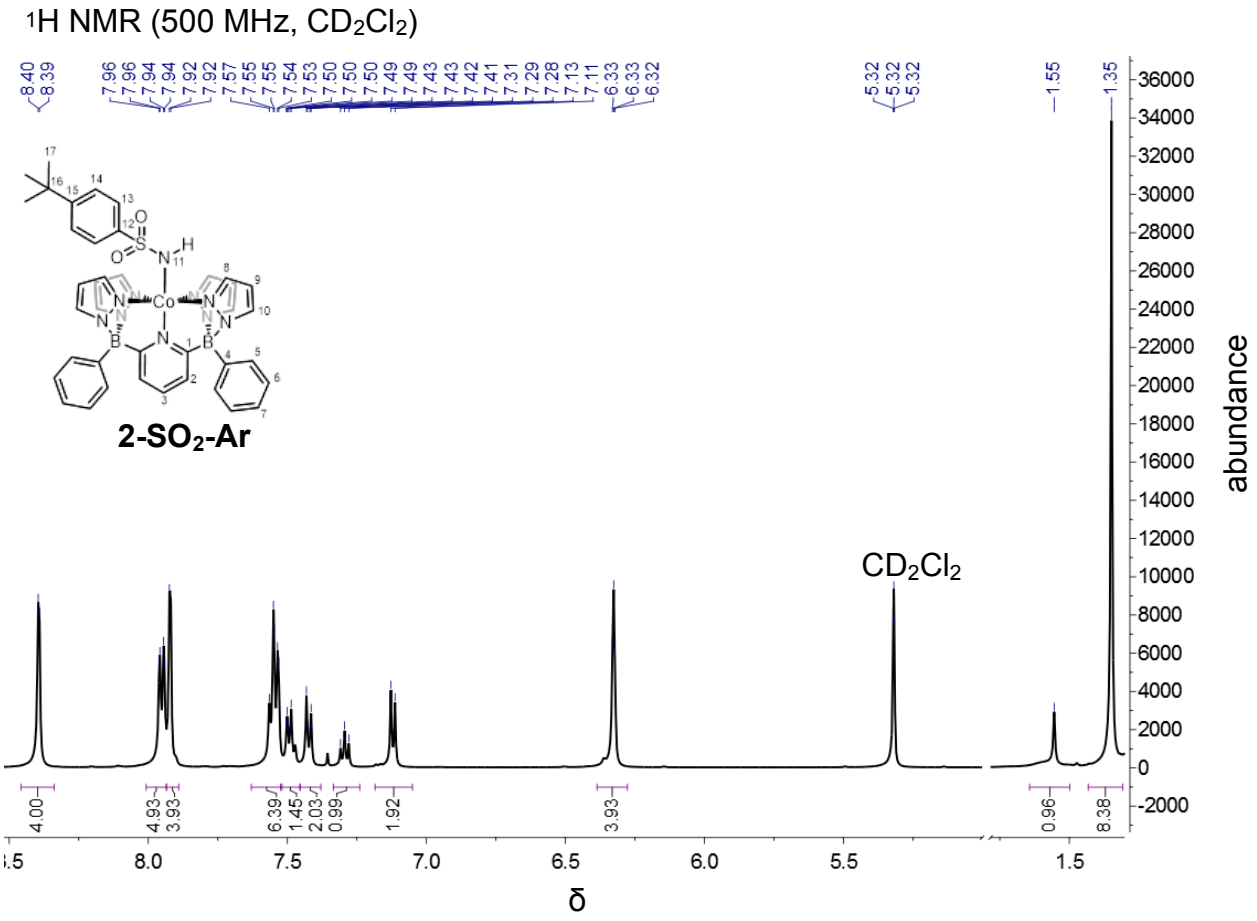

Figure S19. ^{1}H NMR spectrum of **2-SO$_2$-Ar** in CD_2Cl_2.

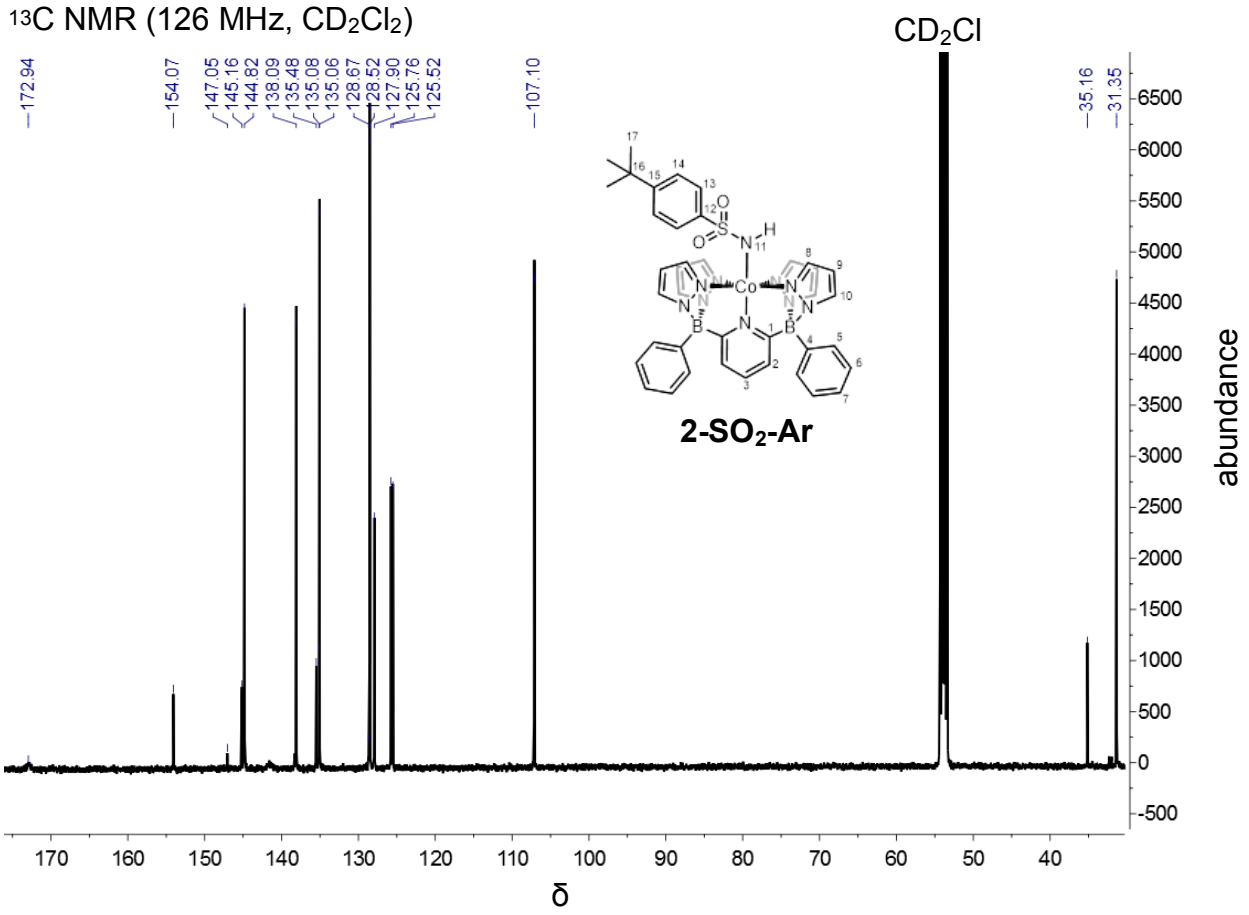

Figure S20. ^{13}C NMR spectrum of **2-SO_2-Ar** in CD_2Cl_2.

^{1}H NMR (500 MHz, C_6D_6)

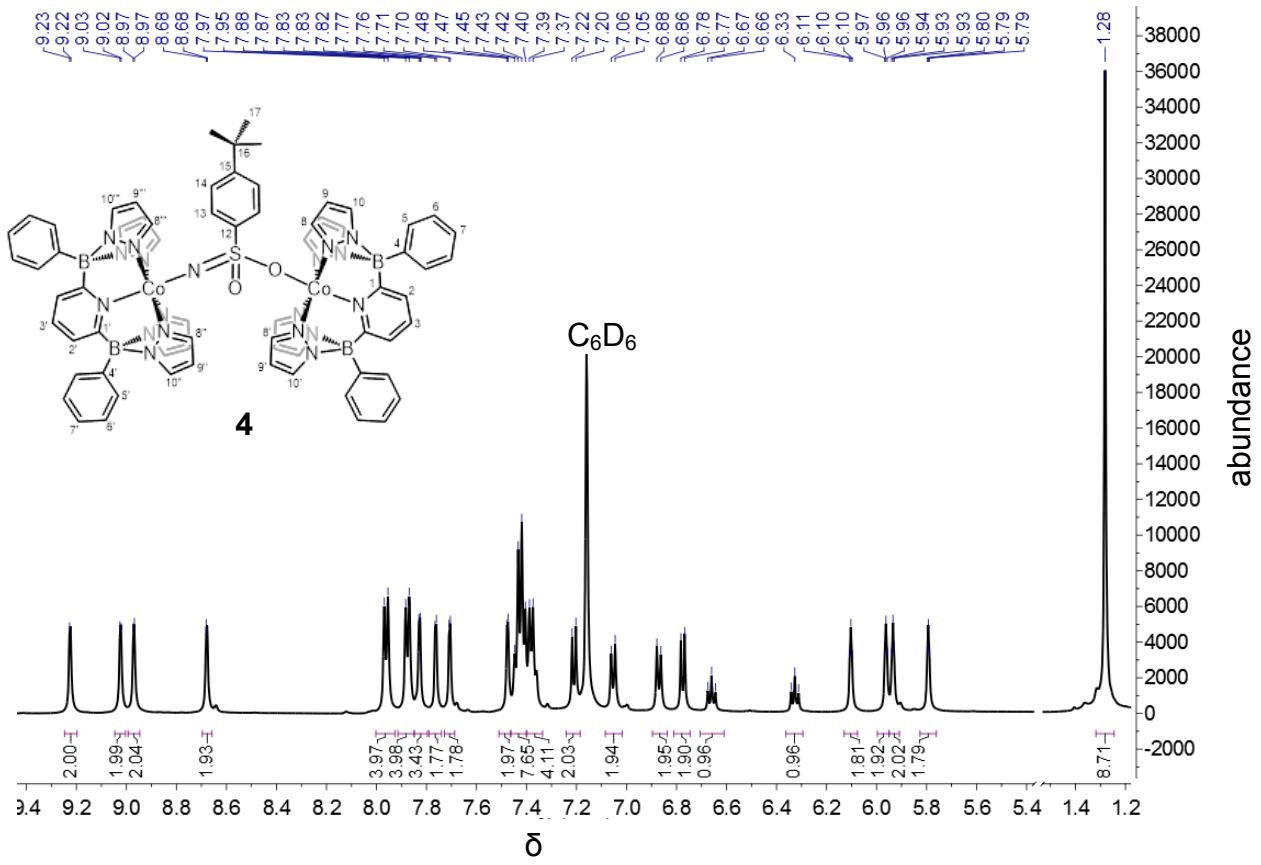

Figure S21. ^{1}H NMR spectrum of **4** in C_6D_6.

$^{13}C\{^{1}H\}$ NMR (126 MHz,

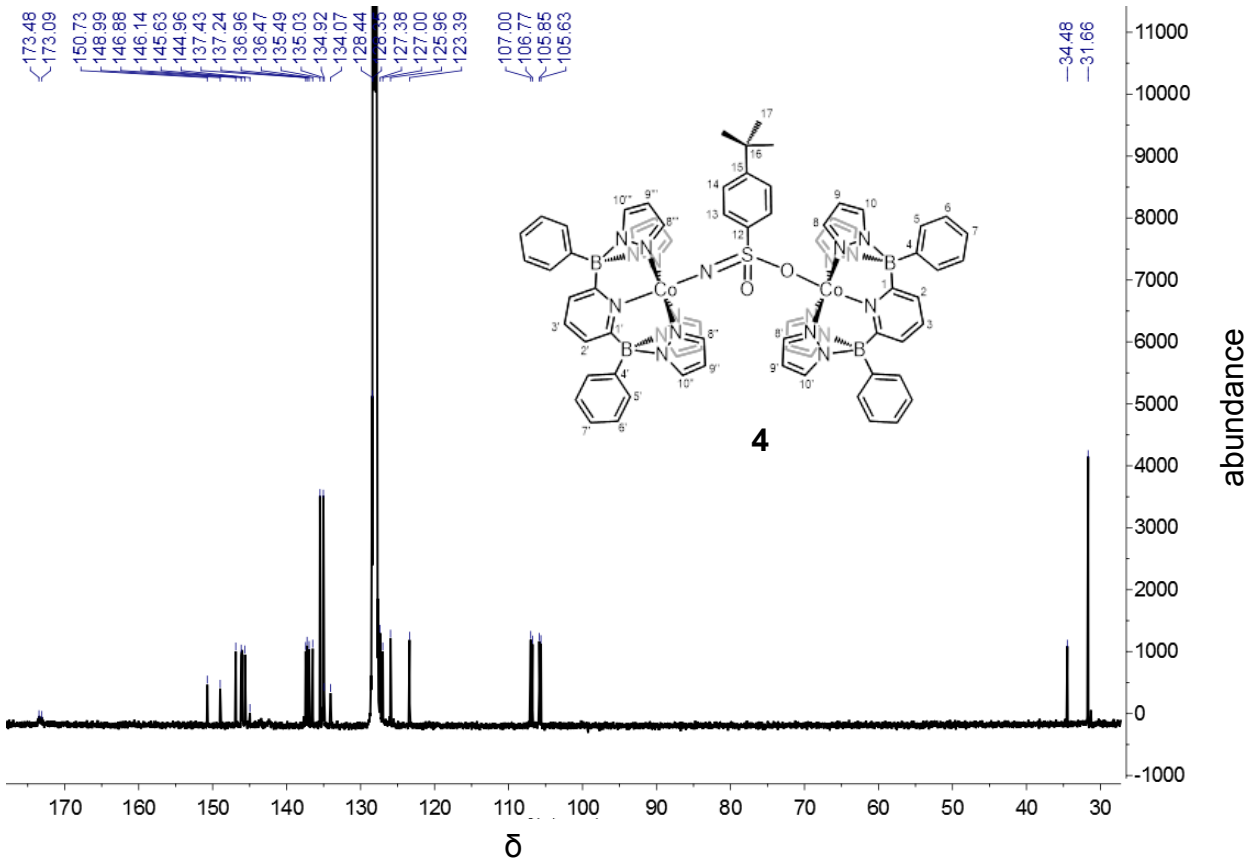

Figure S22. $^{13}C\{^{1}H\}$ NMR spectrum of **4** in C_6D_6.

Table S1. List of structurally characterized cobalt(III) amido complexes found in the literature.

Compound	C.N.	Co-N_{amido}	Reference
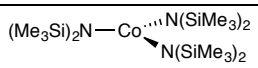	3	1.870(3)	Power[10]
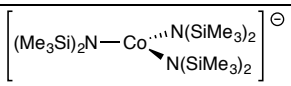	3	1.975(2) 1.981(2) 1.973(2)	Dehnicke[11]
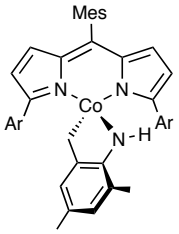	4	1.848(4)	Betley[12]
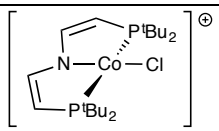	4	1.8518(11) 1.8552(11)	Schneider[13]
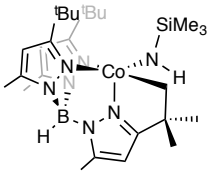	5	1.893(3)	Theopold [14]
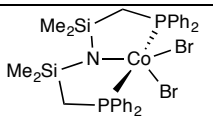	5	1.926(5)	Fryzuk[15]
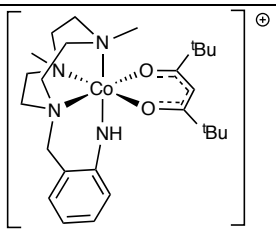	6	1.912(6)	Wieghart[16]

Table S2. Crystal Data Collection and Refinement Parameters for Compounds**, 1-THF, and 1.**

	1-THF	**1**
chemical formula	$C_{33}H_{25}B_2CoN_9O$	$C_{29}H_{25}B_2CoN_9, C_6H_6$
crystal colour	Peach	Brown
***Fw*; *F*(000)**	1294.38; 2672	658.24; 2728
***T* (K)**	173(2)	100(2)
wavelength (Å)	1.54178	0.71073
space group	Pnma	$P2_1$
***a* (Å)**	13.985(1)	13.846(3)
***b* (Å)**	22.079(2)	14.677(3)
***c* (Å)**	19.893(2)	30.879(6)
α (deg)	90	90
β (deg)	90	99.64(5)
γ (deg)	90	90
Z	4	8
***V* (Å^3)**	6142(1)	6187(2)
ρ_{calcd} (g·cm^{-3})	1.400	1.413
μ (mm^{-1})	4.732	0.598
θ range (deg); completeness	2.990 − 66.888; 0.979	1.492 to 24.999; 0.986
collected reflections; R_σ	39148; 0.0568	20479; 0.0629
unique reflections; R_{int}	39148; 0.0907	20479; 0.0473
R1[a]; wR2[b] [I > 2σ(I)]	0.0456; 0.1240	0.0660; 0.1356
R1; wR2 [all data]	0.0579; 0.1339	0.0768; 0.1427
GOF	1.020	1.173
largest diff peak and hole	0.473 and -0.356	0.671 and -0.335

Table S3. Crystal Data Collection and Refinement Parameters for Complexes **2-tBu**, **2-SO_2Ar**, **and 2-CF_3**.

	2-tBu	**2-SO_2Ar**	**2-CF_3**
chemical formula	$C_{39}H_{39}B_2CoN_{10}$, 0.5 C_6H_6	$C_{39}H_{39}B_2CoN_{10}O_2S$, C_6H_6	$C_{37}H_{29}B_2CoF_6N_{10}$,2 C_6H_6
crystal colour	Forest green	Pink	Green
***Fw*; *F*(000)**	767.40; 6416	870.52; 1816	964.47; 1984
***T* (K)**	100(2)	173(2)	173
wavelength (Å)	0.71073	1.54178	0.68881
space group	Fdd2	P-1	Pnma
***a* (Å)**	68.484(4)	16.9567(8)	20.228(4)
***b* (Å)**	27.6660(14)	17.0890(8)	9.862(2)
***c* (Å)**	7.9665(4)	18.2890(8)	22.726(5)
α (deg)	90	116.702(2)	90
β (deg)	90	105.312(2)	90
γ (deg)	90	99.447(2)	90
Z	16	4	4
***V* (Å^3)**	15094.0(14)	4313.5(4)	4533.6(16)
ρ_{calcd} (g·cm^{-3})	1.351	1.340	1.413
μ (mm^{-1})	0.501	3.975	0.413
θ range (deg); completeness	1.893 to 24.984; 0.996	2.860 − 67.500; 0.947	1.306 − 24.999;
collected reflections; R_σ	29101; 0.0846	40230; 0.0733	61203; 0.0366
unique reflections; R_{int}	29101; 0.1571	14736; 0.0578	4474; 0.0792
R1[a]; wR2[b] [I > 2σ(I)]	0.0855; 0.1796	0.0519; 0.1157	0.0563; 0.1489
R1; wR2 [all data]	0.1024; 0.1926	0.0803; 0.1302	0.0579; 0.1504
GOF	1.215	1.027	1.092
largest diff peak and hole	0.593 and -0.709	0.338 and -0.368	0.913 and -0.849

Table S4. Crystal Data Collection and Refinement Parameters for Complexes **4** and **3-CF$_3$**.

	4	**3-CF$_3$**
chemical formula	$C_{68}H_{63}B_4Co_2N_{19}O_2S$, C_6H_6	$C_{74}H_{56}B_4Co_2F_{12}N_{20}$, C_6H_6
crystal colour	Purple	Green
***Fw*; *F*(000)**	1449.64, 1504	1692.59, 3456
***T* (K)**	100(2)	173
wavelength (Å)	0.71073	0.77491
space group	P-1	P21/c
***a* (Å)**	13.160(3)	17.209(3)
***b* (Å)**	16.563(3)	17.274(3)
***c* (Å)**	17.625(4)	31.426(9)
α (deg)	102.21(3)	90
β (deg)	109.90(3)	119.69(2)
γ (deg)	94.97(3)	90
Z	2	4
***V* (Å^3)**	3477.6(15)	8116(3)
ρ_{calcd} (g·cm^{-3})	1.384	1.385
μ (mm^{-1})	0.570	0.618
θ range (deg); completeness	2.543 to 25.000; 0.989	1.521 − 26.998; 0.987
collected reflections; R_σ	22380; 0.0450	66096; 0.0380
unique reflections; R_{int}	22380; 0.0365	13488; 0.0525
R1[a]; wR2[b] [I > 2σ(I)]	0.0478; 0.0963	0.0609; 0.1589
R1; wR2 [all data]	0.0625; 0.1060	0.0801; 0.1712
GOF	1.075	1.057
largest diff peak and hole	0.799 and -0.488	0.680 and -0.794

References.

1. Lee, W.-T.; Dickie, D. A.; Metta-Magaña, A. J.; Smith, J. M. A Tripodal Ligand Constructed from Mesoionic Carbene Donors. *Inorg. Chem.* **2013,** 52, 12842-12846.
2. Bettinger, H. F.; Filthaus, M.; Bornemann, H.; Oppel, I. M. Metal-Free Conversion of Methane and Cycloalkanes to Amines and Amides by Employing a Borylnitrene. *Angew. Chem. Int. Ed.* **2008,** 47, 4744-4747.
3. Laitar, D. S.; Mathison, C. J. N.; Davis, W. M.; Sadighi, J. P. Copper(I) Complexes of a Heavily Fluorinated β-Diketiminate Ligand: Synthesis, Electronic Properties, and Intramolecular Aerobic Hydroxylation. *Inorg. Chem.* **2003,** 42, 7354-7356.
4. Becke, A. D. Density-functional thermochemistry. III. The role of exact exchange. *J. Chem. Phys.* **1993,** 98, 5648-5652.
5. Perdew, J. P.; Wang, Y. Accurate and simple analytic representation of the electron-gas correlation energy. *Phys. Rev. B* **1992,** 45, 13244-13249.
6. Dolg, M.; Wedig, U.; Stoll, H.; Preuss, H. Energy-adjusted ab initio pseudopotentials for the first row transition elements. *J. Chem. Phys.* **1987,** 86, 866-872.
7. Hehre, W. J.; Ditchfield, R.; Pople, J. A. Self—Consistent Molecular Orbital Methods. XII. Further Extensions of Gaussian—Type Basis Sets for Use in Molecular Orbital Studies of Organic Molecules. *J. Chem. Phys.* **1972,** 56, 2257-2261.
8. Hariharan, P. C.; Pople, J. A. The influence of polarization functions on molecular orbital hydrogenation energies. *Theoretical Chemistry Accounts: Theory, Computation, and Modeling (Theoretica Chimica Acta)* **1973,** 28, 213-222.
9. Gale, R. J.; Osteryoung, R. A. Electrochemical Reduction of Pyridinium Ions in Ionic Aluminum Chloride: Alkylpyridinium Halide Ambient Temperature Liquids. *J. Electrochem. Soc.* **1980,** 127, 2167-2172.
10. Ellison, J. J.; Power, P. P.; Shoner, S. C. First examples of three-coordinate manganese(III) and cobalt(III): synthesis and characterization of the complexes M[N(SiMe3)2]3 (M = Mn or Co). *J. Am. Chem. Soc.* **1989,** 111, 8044-8046.
11. Putzer, M. A.; Neumüller, B.; Dehnicke, K.; Magull, J. Synthese und Kristallstrukturen der Amido-Komplexe [Na(12-Krone-4)2][M{N(SiMe3)2}3] mit M = Mn, Fe und Co. *Chem. Ber.* **1996,** 129, 715-719.
12. King, E. R.; Sazama, G. T.; Betley, T. A. Co(III) Imidos Exhibiting Spin Crossover and C–H Bond Activation. *J. Am. Chem. Soc.* **2012,** 134, 17858-17861.
13. Lagaditis, P. O.; Schluschaß, B.; Demeshko, S.; Würtele, C.; Schneider, S. Square-Planar Cobalt(III) Pincer Complex. *Inorg. Chem.* **2016,** 55, 4529-4536.
14. Thyagarajan, S.; Shay, D. T.; Incarvito, C. D.; Rheingold, A. L.; Theopold, K. H. Intramolecular C−H Activation by Inferred Terminal Cobalt Imido Intermediates. *J. Am. Chem. Soc.* **2003,** 125, 4440-4441.
15. Fryzuk, M. D.; Leznoff, D. B.; Thompson, R. C.; Rettig, S. J. One-Electron Transformations of Paramagnetic Cobalt Complexes. Synthesis and Structure of Cobalt(II) Amidodiphosphine Halide and Alkyl Complexes and Their Reaction with Alkyl Halides. *J. Am. Chem. Soc.* **1998,** 120, 10126-10135.
16. Penkert, F. N.; Weyhermüller, T.; Bill, E.; Hildebrandt, P.; Lecomte, S.; Wieghardt, K. Anilino Radical Complexes of Cobalt(III) and Manganese(IV) and Comparison with Their Phenoxyl Analogues. *J. Am. Chem. Soc.* **2000,** 122, 9663-9673.